Available online at www.sciencedirect.com
SCIENCE DIRECT®
PERGAMON
International Journal of Heat and Mass Transfer 46 (2003) 1529–1539
International Journal of HEAT and MASS TRANSFER
www.elsevier.com/locate/ijhmt

Large eddy simulation of turbulent channel flow with mass transfer at high-Schmidt numbers

Yu-Hong Dong, Xi-Yun Lu *, Li-Xian Zhuang

Department of Modern Mechanics, University of Science and Technology of China, Hefei, Anhui 230026, People's Republic of China

Received 10 June 2002; received in revised form 22 October 2002

Abstract

Large eddy simulation (LES) of turbulent channel flow with mass transfer has been performed to investigate the effect of the Schmidt number on the turbulence behaviors. The three-dimensional filtered Navier–Stokes equations and the concentration equation are numerically solved using a fractional-step method. Dynamic subgrid-scale (SGS) models for the turbulent SGS stresses and mass fluxes are employed to closure the governing equations. The objectives of this study are to examine the reliability of the LES technique for predicting the turbulent mass transfer at high-Schmidt numbers and to analyze the behavior of turbulent mass diffusion from a solid boundary to the adjacent shear flow at different Schmidt numbers. Fully developed turbulent channel flows with constant difference of concentrations imposed on different walls are calculated for a wide range of the Schmidt number from 0.1 up to 200 and the Reynolds number 13 800 based on the centerline mean velocity and the half-width of the channel. To show the effects of Schmidt number on the turbulent mass transfer, mean and fluctuating resolved concentrations, mass transfer coefficient, turbulent mass fluxes, and some instantaneous flow and concentration fields are exhibited and analyzed.

Keywords: Large eddy simulation; Turbulent channel flow; Turbulent mass transfer

1. Introduction

Turbulent mass and heat transfer from wall or between two solid boundaries are of great interest in a variety of engineering applications. Experimental and numerical studies have been performed to investigate this problem at various Reynolds (Re) and Schmidt (Sc) numbers. However, very few results in the literature were concerned with the concentration fluctuations and velocity–concentration correlations in the mass transfer of the turbulent boundary layer, in particular, at high-Schmidt number. For a better understanding of the mechanisms controlling the turbulent mass transfer from a rigid boundary, it is helpful to examine the concentration and velocity fluctuations and their correlations simultaneously.

In the problem of mass transfer by fluid flow, the Schmidt number can be ranged from order of unity or less for gaseous substances in air, to hundreds for salinity in water, and to thousands for color dyes in water. Such problems can be described by the concentration variable that is solely advected by the fluid and transported by the random motion of micro-particles, but which is neither created nor destroyed within the flow and does not directly affect the flow field. The fundamental mechanism and main statistical characteristics of the fluctuating mass transfer need to be investigated in detail. In the case of the mass transfer at low or moderate Schmidt numbers, a significant concentration gradient exists not only in the diffusive sublayer but also in the region outside the sublayer. High-Schmidt number mass transfer is of special importance in the understanding of the mass transfer in a turbulent boundary layer flow. The mass diffusive sublayer for the high-Schmidt number mass transfer by the rigid boundary is very thin, and the mass transfer efficiency is primarily controlled by turbulent motions very closing to the wall.

* Corresponding author. Tel.: +86-551-3601542; fax: +86-551-3606459.
E-mail address: xlu@ustc.edu.cn (X.-Y. Lu).

0017-9310/03/$ - see front matter
PII: S0017-9310(02)00456-8

Nomenclature

C	concentration
$\overline{C}$	resolved concentration
C'	resolved concentration fluctuation
C_δ	concentration on the upper wall
$C_{-\delta}$	concentration on the bottom wall
C_τ	friction concentration
D	molecular diffusivity
G	SGS model coefficient
K_C^+	turbulent mass transfer coefficient
$\bar{p}$	resolved modified pressure
Pr	Prandtl number
q_i	SGS turbulent mass flux
Re	Reynolds number
$\overline{S}_{ij}$	resolved strain rate tensor
Sc	Schmidt number
Sc_T	turbulent Schmidt number
t	time
U_m	centerline mean velocity of the channel
u	resolved streamwise velocity component
$\bar{u}_i$	resolved velocity components
u_i'	velocity fluctuations
u_τ	friction velocity
v	resolved wall-normal velocity component
w	resolved spanwise velocity component
x_i	Cartesian coordinate axes
y	wall-normal coordinate
δ	half-width of the channel
δ_C^+	thickness of diffusive sublayer
$\overline{\Delta}$	size of grid filter
$\widehat{\Delta}$	size of test filter
τ_{ij}	SGS turbulent stress tensor
ν	molecular kinematic viscosity
$\langle\ \rangle$	time and spatial averaging

Subscripts

rms	root mean square
min	minimum

Superscript

$+$	normalized quantity by wall parameters

The complexity of turbulence interactions near the wall results in unusual behaviors of the concentration fluctuations. Thus it is a challenging task to study the mass transfer at high-Schmidt numbers.

Many efforts have been devoted to the experimental investigation and numerical simulation of this problem. Buch and Dahm [1,2] and Shaw and Hanratty [3] experimentally studied the small-scale structure of conserved scalar fields in turbulent shear flows for the cases of $Sc \gg 1$ and $Sc \approx 1$. Kader and Yaglom [4] studied the laws of mass transfer for fully developed turbulent wall flows. In the numerical simulation, it is necessary to accurately calculate and analyze the concentration and velocity fluctuations near the wall. The numerical calculation, in particular, the direct numerical simulation (DNS) can reasonably predict the fluctuating quantities, the correlations of the fluctuations, the structures of the concentration field, and the scalar spectrum. However, because of the expensive cost of DNS, the previous work based on DNS was only limited to low-Schmidt and low- to medium-Reynolds flows. Yeung et al. [5] used the DNS to study the mass diffusion with Sc up to 4. Similar studies on passive heat transfer with the Prandtl number $Pr < 10$ by turbulent flow were reported in [6–10]. Lyons et al. [11,12] also studied the passive heat transfer between the walls of a channel at the Prandtl number unity. However, it is almost impossible to solve those problems, in which both the Reynolds and Schmidt numbers are high, using the DNS since the number of mesh points required to describe all the concentration scales is of order $Sc^3Re^{9/4}$. So, the limitation of the grid resolution has restricted the DNS to low values of the Schmidt number.

It is now well established that large eddy simulation (LES) technique, which is much cheaper than DNS since it solves only the large-scale components of turbulent flow and models the subgrid-scales (SGS) effects via SGS models, provides an efficient tool to study the detailed features of turbulent flows. In the LES, the SGS model plays a key role. A dynamic SGS model was proposed by Germano et al. [13,14] which overcomes some intrinsic drawbacks of the classical Smagorinsky model. The dynamic model received a large success in the past years and it gave a new impetus on the applications and developments of new strategies for the LES. This approach was also extended to the compressible turbulence by Moin et al. [15]. Later, Wang and Pletcher [16] used this compressible version to investigate the turbulent flow in a channel with significant heat transfer. Calmet and Magnaudet [17] used the dynamic mixed model proposed by Zang et al. [18] to carry out the calculation of mass transfer in a turbulent channel flow. In addition, linear eddy model was used by Chakravarthy and Menon [19] to study Reynolds and Schmidt number effects on the turbulent scalar mixing. Those studies make a highly tempting to use dynamic SGS models for studying high-Schmidt-number mass transfer near rigid boundaries.

Usually, a fully developed turbulent channel flow is used as a typical flow because of its simple geometry and

fundamental nature in understanding the mass transfer between fluid and solid walls. In this paper, LES technique is employed to investigate the fully developed turbulent channel flow with the mass transfer. The three-dimensional resolved incompressible Navier–Stokes equations and the concentration equation are solved simultaneously by the fractional-step method proposed by Kim and Moin [20]. Dynamic SGS models for SGS turbulent stresses and turbulent mass fluxes are used to closure the equations. Some typical quantities are discussed based on the present LES calculation.

This paper is organized as follows. The mathematical formulation and the dynamic SGS model for the turbulent stresses and mass fluxes are described in Section 2. Numerical method is briefly given in Section 3. In Section 4, some relevant quantities including mean and fluctuating resolved concentrations, mass transfer coefficient, and turbulent mass flux are discussed. Finally, concluding remarks are given in Section 5.

2. Governing equations

Numerical solutions are obtained by solving the three-dimensional, time-dependent filtered incompressible Navier–Stokes equations and concentration equation simultaneously. To non-dimensionalize the governing equations, as shown schematically in Fig. 1, the half-width δ of the channel is used as the length scale, the mean velocity U_m at the central line as the velocity scale, and the difference of concentration between the upper and lower walls ΔC as the concentration scale. Then the non-dimensional governing equations are given as

$$\frac{\partial \bar{u}_i}{\partial x_i} = 0 \tag{1}$$

$$\frac{\partial \bar{u}_i}{\partial t} + \frac{\partial}{\partial x_j}(\bar{u}_i \bar{u}_j) = -\frac{\partial \bar{p}}{\partial x_i} + \frac{1}{Re}\frac{\partial^2 \bar{u}_i}{\partial x_j \partial x_j} - \frac{\partial \tau_{ij}}{\partial x_j} \tag{2}$$

$$\frac{\partial \overline{C}}{\partial t} + \frac{\partial}{\partial x_j}(\overline{C}\bar{u}_j) = \frac{1}{ReSc}\frac{\partial^2 \overline{C}}{\partial x_j \partial x_j} - \frac{\partial q_j}{\partial x_j} \tag{3}$$

where $\tau_{ij} = R_{ij} - \delta_{ij}R_{kk}/3$, $R_{ij} = \overline{u_i u_j} - \bar{u}_i\bar{u}_j$, $q_j = \overline{Cu}_j - \overline{C}\bar{u}_j$, overbar "–" represents the resolved variable, the Reynolds number Re is defined as $Re = U_m\delta/\nu$, and the Schmidt number Sc as $Sc = \nu/D$, here ν is the kinematic viscosity and D is the molecular diffusivity of scalar, and $\bar{p}$ is the resolved modified pressure, which contains a term $R_{kk}/3$.

In Eqs. (2) and (3), τ_{ij} and q_j represent SGS turbulent stress and mass flux, respectively, which need to be modeled by SGS models. It is assumed that the mass concentration is a passive scalar that does not influence the flow dynamics. Thus the concentration depends on both Re and Sc independently. The overall expressions of the SGS stresses and the SGS turbulent mass flux read, respectively

$$\tau_{ij} = -2G\overline{\Delta}^2|\overline{S}|\overline{S}_{ij} \tag{4}$$

and

$$q_j = -\frac{G\overline{\Delta}^2}{Sc_T}|\overline{S}|\frac{\partial \overline{C}}{\partial x_j} \tag{5}$$

where

$$\overline{S}_{ij} = \frac{1}{2}\left(\frac{\partial \bar{u}_i}{\partial x_j} + \frac{\partial \bar{u}_j}{\partial x_i}\right), \quad |\overline{S}| = [2\overline{S}_{ij}\overline{S}_{ij}]^{1/2}$$

Here, the model coefficients of G and Sc_T in Eqs. (4) and (5) are determined by use of the approach proposed by Germano et al. [14]. After introducing a test filtering with a filter width $\widehat{\overline{\Delta}}$ to Eqs. (1)–(3), the coefficients G and Sc_T can be dynamically determined, by a least-square approach, as

$$G = -\frac{1}{\overline{\Delta}^2}\frac{\langle L_{ij}M_{ij}\rangle_S}{\langle M_{ij}M_{ij}\rangle_S}, \quad Sc_T = -G\overline{\Delta}^2\frac{\langle F_iF_i\rangle_S}{\langle H_iF_i\rangle_S} \tag{6}$$

where

$$M_{ij} = 2\alpha^2\left|\widehat{\overline{S}}\right|\left[\widehat{\overline{S}}_{ij} - \tfrac{1}{3}\widehat{\overline{S}}_{kk}\delta_{ij}\right] - \hat{m}_{ij},$$
$$m_{ij} = 2|\overline{S}|[\overline{S}_{ij} - \tfrac{1}{3}\overline{S}_{ij}\delta_{ij}]$$

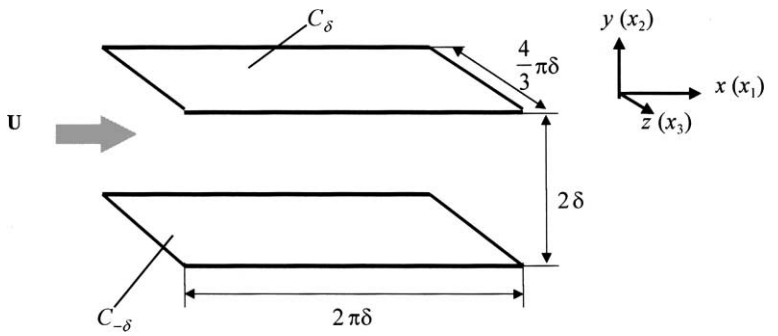

Fig. 1. Sketch of channel flow with mass transfer.

$$L_{ij} = \widehat{\bar{u}_i\bar{u}_j} - \hat{\bar{u}}_i\hat{\bar{u}}_j - \tfrac{1}{3}(\widehat{\bar{u}_k\bar{u}_k} - \hat{\bar{u}}_k\hat{\bar{u}}_k)\delta_{ij}$$

$$H_i = \hat{\bar{u}}_i\widehat{\bar{C}} - \widehat{\bar{u}_i\bar{C}}, \quad F_i = \alpha^2\left|\widehat{\bar{S}}\right|\widehat{\bar{B}}_i - \widehat{|\bar{S}|B_i}, \quad \text{and} \quad B_j = \frac{\partial\bar{C}}{\partial x_j}$$

Here, $\alpha = \widehat{\Delta}/\Delta$ is chosen as 2 in the present calculation, $\langle\rangle_S$ denotes some kind of spatial averaging to remove the calculation oscillation [14]. In the present calculation for turbulent channel flow, the average is taken in the plane parallel to the wall plate since both the flow field and the concentration field are assumed statistically homogeneous in the streamwise and spanwise directions.

In this study, a fully developed turbulent channel flow with mass transfer, as shows in Fig. 1, is calculated. The flow and concentration fields are assumed to be statistically homogeneous in the streamwise (x) and spanwise (z) directions. Thus periodic boundary conditions are employed in those directions. Two different constant concentrations $C_\delta = 0.5$ and $C_{-\delta} = -0.5$ are imposed on the top and bottom walls respectively, which drive the mass transfer. At the walls $y = \pm 1$, no-slip and no-penetration velocity conditions are imposed.

3. Numerical methods

Eqs. (1)–(3) are discretized using the second-order accurate finite-difference scheme for both spatial and temporal derivatives. A staggered grid is used to solve the governing equations. The system of discretized equations is solved by a fractional-step method and the advancement in time is performed by the semi-implicit scheme using the Crank–Nicolson scheme for the viscous terms and three-stage Runge–Kutta scheme for the convective terms. The low-storage Runge–Kutta methods have the additional advantage that they require the minimum amount of computer memory for this class of schemes. Spatial derivatives are approximated by a second-order central difference. The relevant discretized formulation was described in detail by Verzicco and Orlandi [21] and Verzicco and Camussi [22].

4. Results and discussion

In the present study, the Schmidt number is chosen from 0.1 to 200 and the Reynolds number based on the centerline mean velocity and the half-width of the channel is 13 800. The computational domain is $2\pi\delta$, 2δ and $4\pi\delta/3$ with corresponding grid number being $65 \times 97 \times 65$, in the streamwise (x), wall-normal (y) and spanwise (z) directions, respectively. The chosen computation domain ensures that the two-point correlations separated by those length scales in the streamwise and spanwise directions are negligibly small. The grid independence of the computational results has been checked in advance. The grid is uniform along x- and z-directions. In the wall-normal direction (y), to increase the grid resolution near both the walls, the mesh size is stretched following the transformation used by Moin and Kim [23,24]

$$y_j = \frac{1}{a}\tanh[\xi_j\tanh^{-1}(a)] \tag{7}$$

where $\xi_j = 1 + 2(j-1)/(N-1)$ and $j = 1, \ldots, N$. The value of a is selected so that the grid distribution in the y-direction is sufficient to resolve the viscous sublayer and diffusive sublayer near the boundary. Therefore, the larger the Schmidt number is, the larger the parameter a ($0 < a < 1$) should be. The minimum mesh sizes $\Delta y^+_{\min} = 0.43$, 0.32, 0.21 and 0.16 are here used for $Sc = 1$, 10, 100 and 200, respectively. Mass transfer computation is started after the flow field has reached a fully developed turbulent state. Initial concentration field is set to be a linear distribution along the y-direction and homogeneous in the horizontal planes.

To validate quantitatively the present calculation, a fully developed turbulent channel flow is calculated at $Re = 13\,800$, which has been repeatedly used in the LES and DNS literature [17,24]. The root mean square (rms) values of the resolved streamwise, spanwise and wall-normal velocity fluctuations, normalized by the friction velocity, are shown in Fig. 2 and compared with the previous LES results given by Calmet and Magnaudet [17]. The streamwise component $u^+_{\rm rms}$ reaches its maximum at $y^+ \approx 14$ and the maximum value is 3.3, which is in very good agreement with the computational results given in [23,24] (not shown here) and slightly deviates the value of 3.2 given by [17]. The maximal values of fluctuations of the spanwise velocity ($w^+_{\rm rms}$) and the wall-normal velocity ($v^+_{\rm rms}$) are 1.0 and 0.9 approximately, in

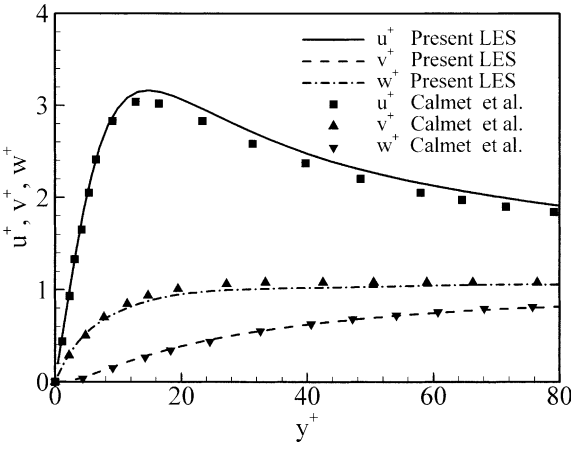

Fig. 2. Distributions of resolvable turbulent intensities along the streamwise, spanwise and wall-normal directions in the wall region.

good agreement with the measurements of Kreplin and Eckelmann [25]. The present computational code has also been verified by our previous studies [26–28]. Thus, it can be confirmed that our calculation is reliable for the prediction of statistical quantities of the turbulent flow and mass transfer.

To depict the behavior of the turbulent mass transfer in the vicinity of the wall, the mean concentration near the bottom wall, i.e., $\langle C^+\rangle = [\langle C(y)\rangle - C(-1)]/C_\tau$, is plotted in Fig. 3 versus $y^+ = (y+1)u_\tau/\nu$ in logarithmic scale, where u_τ represents the friction velocity, $\langle\ \rangle$ denotes an averaging in the plane parallel to the wall plate and in time, and C_τ is defined as

$$C_\tau = \frac{D}{u_\tau}\left(\frac{\partial\langle\overline{C}\rangle}{\partial y}\right)\Big|_{y=-\delta} \tag{8}$$

It is seen that higher concentration appears at larger Schmidt number in the vicinity of the wall. Similar to the mean velocity distribution, there exists a buffer layer followed by a logarithmic region in the mean concentration profile, where, $\langle C^+\rangle$ behaves as

$$\langle C^+\rangle = \alpha \ln y^+ + \beta(Sc) \tag{9}$$

Kader and Yaglom [4] found $\alpha = 2.12$ approximately while Kader [29] gave an empirical expression for the function $\beta(Sc)$ that describes the experimental results in the logarithmic region of the fully turbulent boundary layer. The curves of (9) are plotted in Fig. 3. It is interesting to note that, as expected, the slope of α is approximately constant for $Sc = 0.3$, 1 and 10, almost independent of the Schmidt number. This means that the y^+-logarithmic plots of the mean concentration profile may be nearly parallel for different Sc numbers, which was also confirmed by Kawamura et al. [7] based on DNS calculations.

Within the diffusive sublayer near the boundary, Shaw and Hanratty [3] theoretically suggested a relation between the non-dimensional thickness δ_C^+ of the mass diffusive sublayer and its dynamic equivalent δ_u^+ through the Schmidt number,

$$\delta_C^+ = Sc^{-1/3}\delta_u^+ \tag{10}$$

To illustrate the behavior of the diffusive sublayer, mean velocity and concentration profiles at $Sc = 1$ are shown in Fig. 4, where the velocity and concentration are normalized by u_τ and C_τ defined in (8), respectively. As shown in Fig. 4, it can be identified that $\delta_C^+ = \delta_u^+$, in agreement with Eq. (10) at $Sc = 1$. In Fig. 4, the mean concentration data calculated by Calmet et al. [17] is also plotted and compared well with the present results.

Fig. 5 shows the profile of the mean concentration at $Sc = 100$ in the near wall region. It is seen that the mean concentration profile exhibits a buffer layer followed by a logarithmic region in accordance with the relation (9). By checking the mean concentration profiles in Figs. 4 and 5, we can see that the values of the thickness of the diffusive sublayer turn to be quite close to the $Sc^{-1/3}$ dependency predicted by (10). Experimental and computational data by Nagano and Shimada [30] at $Sc = 95$ and $Re = 10^4$ are also given in Fig. 5. Although the parameters Sc and Re in the present calculation are somewhat different from those in [30], both results are still in good agreement with each other.

Fig. 6 shows the global profiles of mean concentration for different Sc numbers from 0.1 to 200. It is seen that the diffusive boundary layer thickness gets thinner and thinner with the increase of the Schmidt number. If we re-normalize the profiles by using C_τ in (8) versus y^+ in the vicinity of the wall, it is easy to find that the values of the diffusive sublayer thickness at different Sc numbers are related approximately by the $Sc^{-1/3}$ law given in

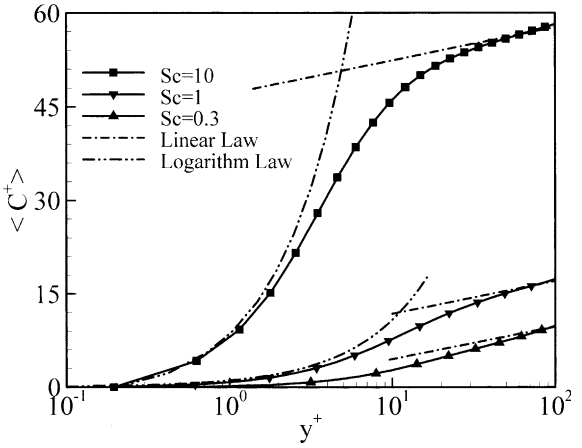

Fig. 3. Profiles of mean resolved concentration for different Schmidt numbers.

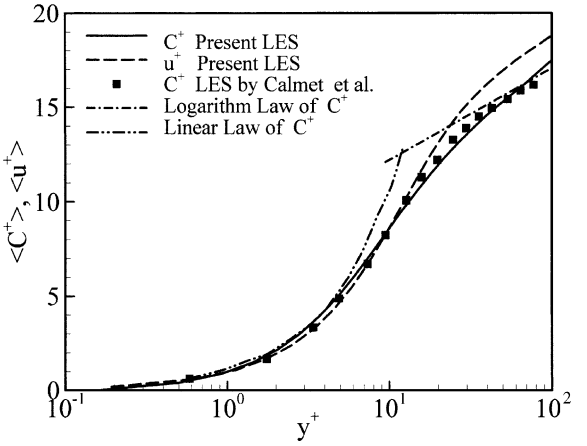

Fig. 4. Distributions of mean resolved concentration and streamwise velocity at $Sc = 1$.

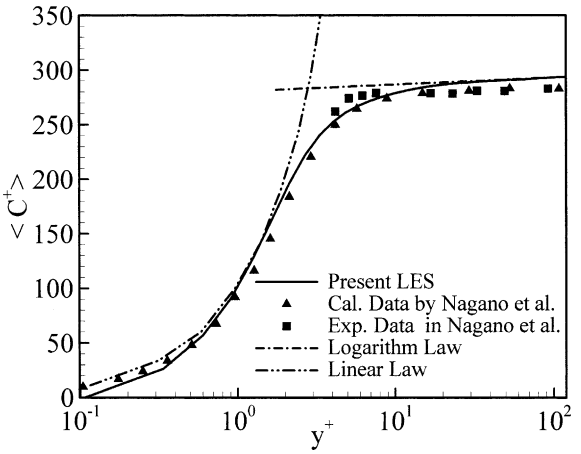

Fig. 5. Profile of mean resolved concentration at $Sc = 100$ and comparison with experimental and computational data.

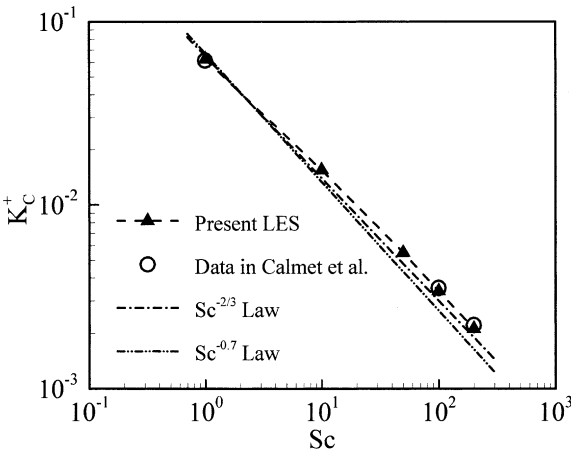

Fig. 7. Distribution of turbulent mass transfer coefficient versus the Schmidt number.

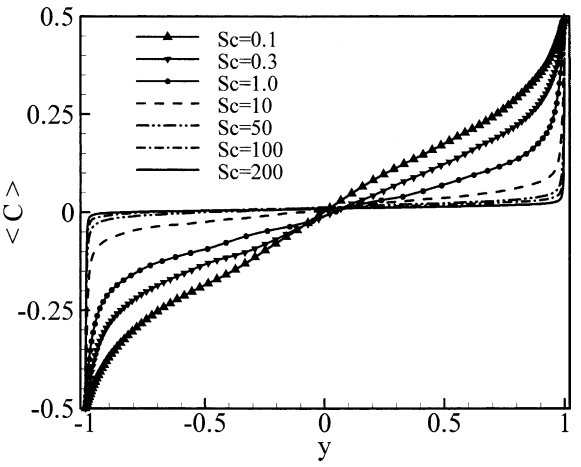

Fig. 6. Profiles of mean resolved concentration for different Schmidt numbers.

(10) and by the $Sc^{-0.3}$ law predicted by the experiment [3].

Now, we discuss the Schmidt number dependence of turbulent mass transfer coefficient K_C^+. The calculated results given by the present study are shown in Fig. 7, and K_C^+ is defined as

$$K_C^+ = \frac{D}{u_\tau \Delta C}\left(\frac{\partial\langle\overline{C}\rangle}{\partial y}\right)\Big|_{y=-1} \tag{11}$$

where ΔC is the difference of concentrations on different walls. Kader and Yaglom [4] suggests the Sc dependence of K_C^+ as $K_C^+ \sim Sc^{-2/3}$ as $Sc \to \infty$. Shaw and Hanratty [3] found $K_C^+ \sim Sc^{-0.7}$ from their experiment. Some data predicted by Calmet et al. [17] is also presented in Fig. 7.

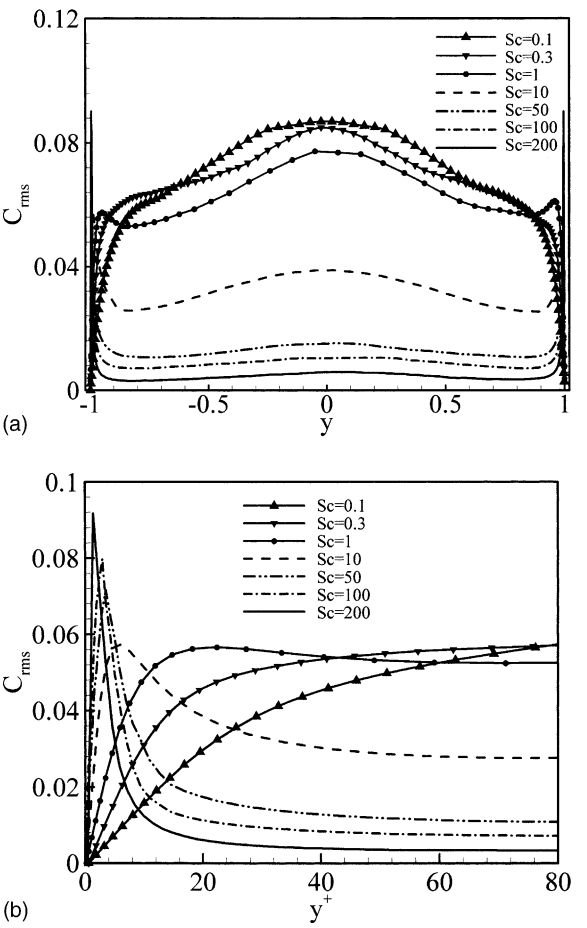

Fig. 8. Profiles of the rms of the resolvable concentration across the channel (a) and close to the wall (b).

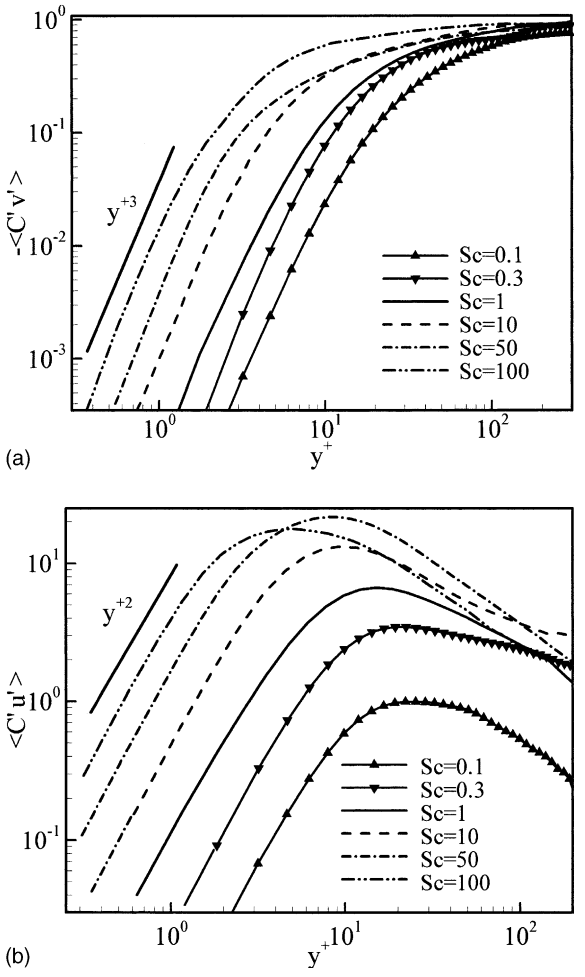

Fig. 9. Distributions of the vertical (a) and streamwise (b) turbulent mass fluxes for different Schmidt numbers.

It can be identified that they are in good agreement with each other.

Fig. 8 shows the profiles of the rms values of the resolvable concentration fluctuation ($C_{\rm rms}$) across the channel (Fig. 8a) and near the wall (Fig. 8b) for $Sc = 0.1$ to 200. At $Sc = 0.1$, 0.3 and 1, the intensity of the fluctuating part of the concentration is high all over the channel. Unlike the velocity fluctuations, the concentration intensity reaches a maximum at the central plane of the channel (Fig. 8a). According to Lyons and Hanratty [11,12], this difference is due to the fact that the different boundary conditions of concentration imposed on different walls cause a non-zero mean concentration gradient in the center of the channel. It is noticed that there is a local extremum in the concentration fluctuation at approximately $y^+ = 17$ from the closest channel wall for $Sc = 1$, which is close to the maximum of the streamwise velocity fluctuation that occurs approximately at $y^+ = 15$, as shown in Fig. 2. As the distance from the wall goes to zero, both the fluctuations of velocity and concentration approach to zero linearly with a slope varying with Sc as shown in Fig. 8b. At $Sc = 50$, 100 and 200, it has been shown that large concentration fluctuations are significant only close to the wall and the maximum of them shifts towards the wall as the Schmidt number increases.

To reveal the character of turbulent mass transfer near the solid walls of a fully developed turbulent channel flow, Figs. 9a and 9b show the variations of the wall-normal and streamwise turbulent mass fluxes versus y^+, respectively, in the wall region for different Schmidt numbers from 0.1 to 100. As the Schmidt number increases, the mass fluxes by turbulent transport $\langle v'C' \rangle$ and $\langle u'C' \rangle$ become increasingly significant in the region near the wall. Furthermore, we can expand $\langle u'C' \rangle$ and $\langle v'C' \rangle$ into power series of y^+ in the vicinity of wall,

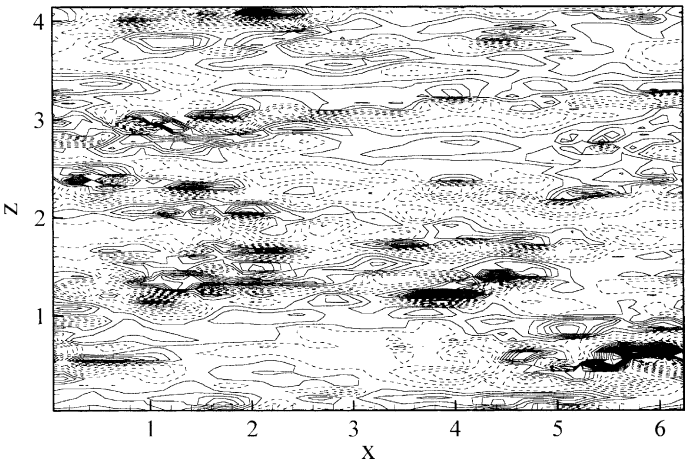

Fig. 10. Contours of instantaneous resolvable streamwise velocity fluctuation field in the (x, z) plane at $y^+ = 1.5$ approximately: Solid lines mean positive values and dashed lines negative values.

$$\langle u'C'\rangle = Sc(f_1 y^{+^2} + f_2 y^{+^3} + \cdots) \quad (12)$$

$$\langle v'C'\rangle = Sc(g_1 y^{+^3} + g_2 y^{+^4} + \cdots) \quad (13)$$

Here, note that $v' = c_1 y^{+^2} + c_2 y^{+^3} + \cdots$, due to $(\partial v'/\partial y)|_{y=\pm\delta} = 0$.

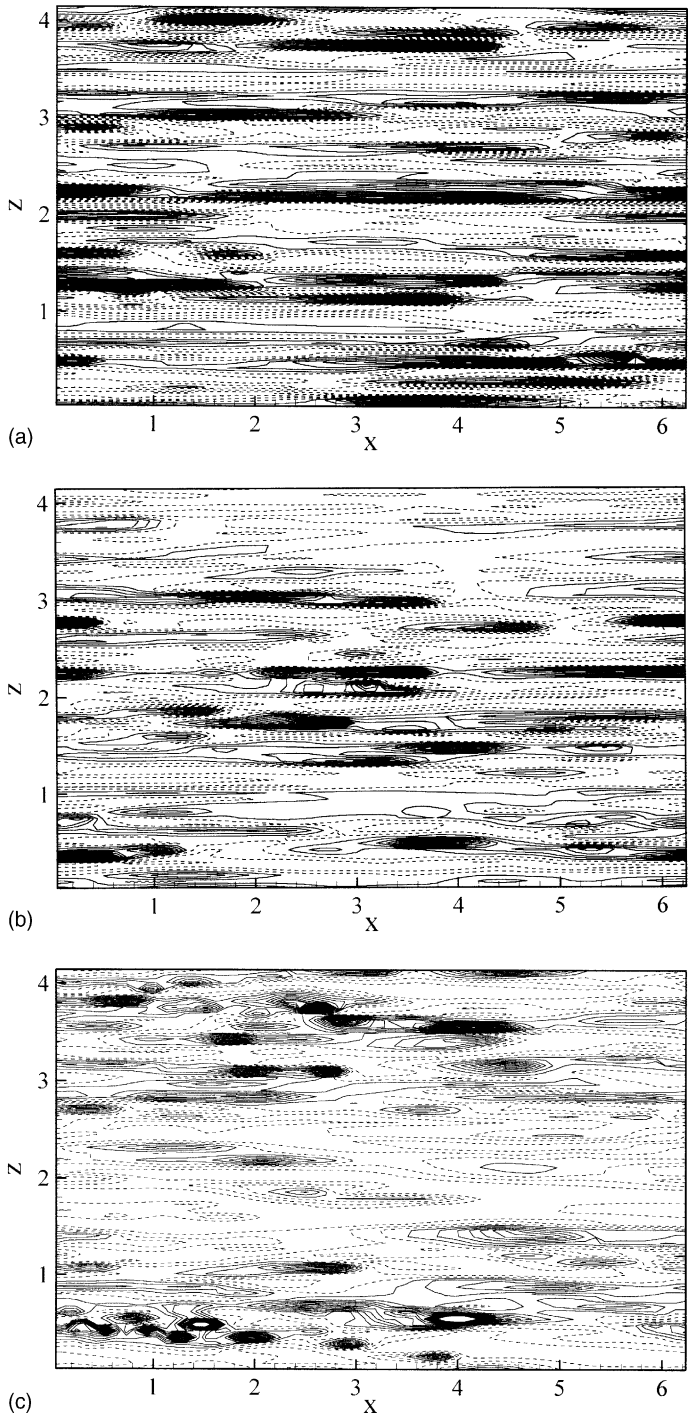

Fig. 11. Contours of instantaneous resolvable concentration fluctuation field in the (x,z) plane at $y^+ = 1.5$ approximately. (a) $Sc = 100$, (b) $Sc = 10$, and (c) $Sc = 1$: Solid lines mean positive values and dashed lines negative values.

Both curves of the square and cubic laws with the wall-normal distance are plotted in Fig. 9 with logarithm scales to illustrate the first terms in (12) and (13). The turbulent mass fluxes in the streamwise and wall-normal directions agree well with the leading term behavior in (12) and (13) in the near wall region, respectively.

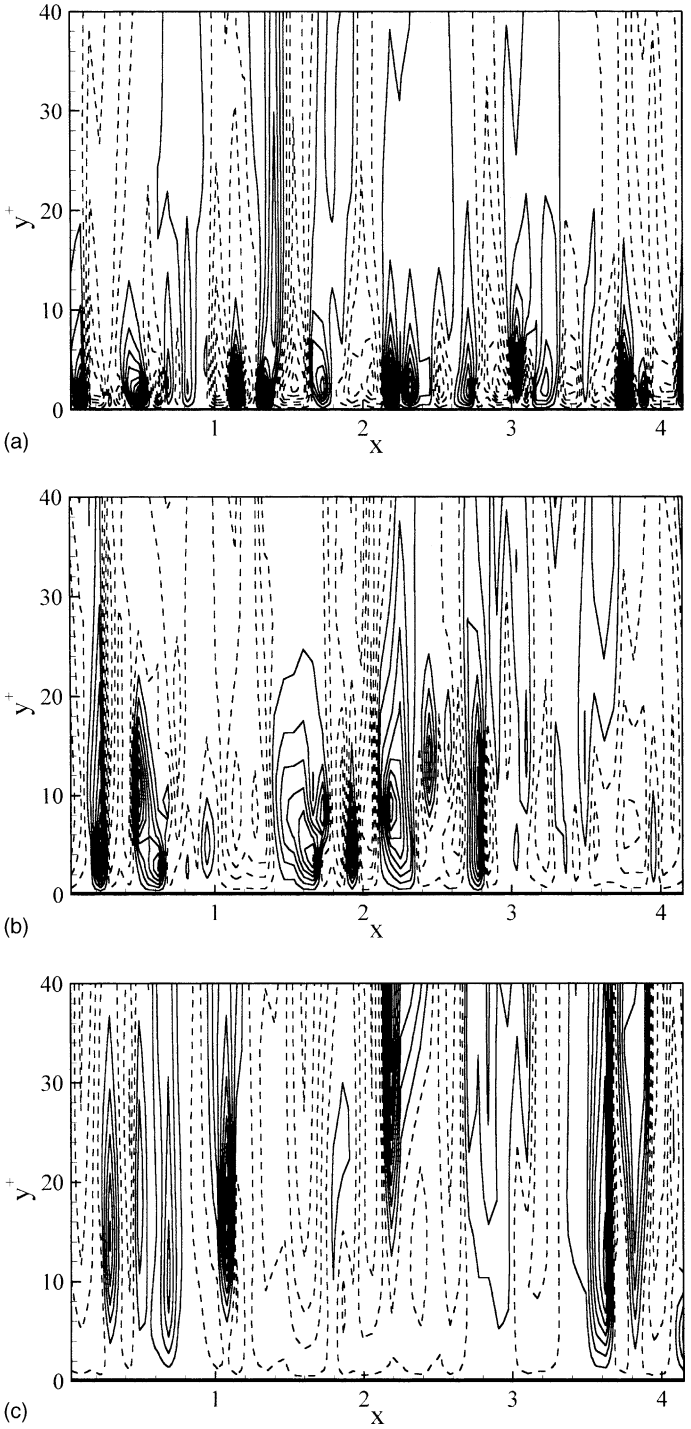

Fig. 12. Contours of the concentration fluctuation in the y^+–z plane. (a) $Sc = 100$, (b) $Sc = 10$, and (c) $Sc = 1$: Solid lines mean positive values and dashed lines negative values.

Fig. 10 shows the structures of instantaneous resolvable streamwise velocity fluctuation field in the (x,z) plane at $y^+ = 1.5$ approximately. The well-known high-speed streaks (dense solid lines) are clearly seen in Fig. 10. Moin and Kim [23] postulated that the wall layer may be viewed as a bed of low-speed fluid that is constantly subjected to the arrival of energetic eddies from the outer layers. These energetic eddies form the high-speed streaks in the wall region. The instantaneous resolvable concentration fluctuation fields in the (x,z) plane are shown in Fig. 11 for $Sc = 1$, 10 and 100. One can identify the local spots in accordance with the high- and low-concentration regions alternately. These observations imply that the turbulent mixing of mass concentration is controlled by the turbulence dynamics in the near wall regions.

Contours of the resolved concentration fluctuation close to the wall in a cross plane (y^+,z) for $Sc = 1$, 10 and 100 are shown in Fig. 12, where the high- and low-concentration streaks are visualized. The organized streaks of the concentration fluctuation exhibit the coherent structures due to the succession of ejection and sweeping events. The vertical size of the closed concentration contours clearly shows that the mass transfer takes place in a much thinner region at $Sc = 100$ than at $Sc = 1$. Consequently, nearly all the turbulent structures existing in the wall region are effective in the mass transfer process at $Sc = 1$, but only the smallest structures subsisting very close to the wall are involved in the transfer process at $Sc = 100$.

5. Concluding remarks

LES of fully developed turbulent channel flow with mass transfer is performed for the Schmidt number from 0.1 up to 200 and the Reynolds number 13 800. The three-dimensional resolved incompressible Navier–Stokes equations and the concentration equation are solved simultaneously using a fractional-step method. Dynamic SGS models for the turbulent stresses and mass fluxes are used to closure governing equations. Statistical turbulence quantities including the mean and fluctuating concentrations, the mass transfer coefficients and the turbulent mass fluxes are obtained and analyzed. The decisive validation of the present approach has been achieved by comparing our calculated results with some available computational, theoretical and experimental results, in particular, for high-Schmidt-number flows. At high-Schmidt number, it has been established that diffusive sublayer thickness δ_C^+ and turbulent mass transfer coefficient K_C^+ behave like $Sc^{-1/3}$ and $Sc^{-2/3}$ as predicted theoretically by Kader and Yaglom [4], or approximately like $Sc^{-0.3}$ and $Sc^{-0.6}$ suggested experimentally by Shaw and Hanratty [3]. The profiles of mean concentration and the concentration fluctuation have been examined in detail. There exists a buffer layer followed by a logarithmic region in the mean concentration profile. At low and medium Schmidt numbers, the concentration fluctuation is high in the whole channel except the wall region. However, at high-Schmidt number, the concentration fluctuation over the central part of the channel is negligibly small because the gradient of mean concentration is nearly zero there. It is also verified that the streamwise and vertical turbulent mass fluxes vary in the manners of y^{+^2} and y^{+^3}, respectively, in the wall vicinity. From the sketches of instantaneous concentration fluctuation contours, it is demonstrated that the mass transfer takes place in a very thin region at high-Schmidt number and only the smallest structures subsisting very close to the wall are involved in the mass transfer process.

Acknowledgements

This work was supported by the National Science Fund for Distinguished Scholars (No. 10125210), the China NKBRSF Project (No. 2001CB409600), and the Hundred Talents Programme of the Chinese Academy of Sciences.

References

[1] K.A. Buch, W.J.A. Dahm, Experimental study of the fine-scale structure of conserved scalar mixing in turbulent shear flows. Part 1. $Sc \gg 1$, J. Fluid Mech. 317 (1996) 21–71.
[2] K.A. Buch, W.J.A. Dahm, Experimental study of the fine-scale structure of conserved scalar mixing in turbulent shear flows. Part 2. $Sc \approx 1$, J. Fluid Mech. 364 (1998) 1–29.
[3] D.A. Shaw, T.J. Hanratty, Turbulent mass transfer rates to a wall for large Schmidt number, AIChE J. 23 (1977) 28–35.
[4] B.A. Kader, A.M. Yaglom, Heat and mass transfer laws for fully turbulent wall flows, Int. J. Heat Mass Transfer 15 (1972) 2329–2342.
[5] P.K. Yeung, M.C. Sykes, P. Vedula, Direct numerical simulation of differential diffusion with Schmidt numbers up to 4.0, Phys. Fluids 12 (2000) 1601–1604.
[6] Y. Na, D.V. Papavassiliou, T.J. Hanratty, Use of direct numerical simulation to study the effect of Prandtl number on temperature field, Int. J. Heat Fluid Flow 20 (1999) 187–195.
[7] H. Kawamura, H. Abe, Y. Matsuo, DNS of turbulent heat transfer in channel flow with respect to Reynolds and Prandtl number effects, Int. J. Heat Fluid Flow 20 (1999) 196–207.
[8] D. Bogucki, J.A. Domaradzki, P.K. Yeung, Direct numerical simulations of passive scalars with $Pr > 1$ advected by turbulent flow, J. Fluid Mech. 343 (1997) 111–130.
[9] Y. Miyake, K. Tsujimoto, M. Nakgi, Direct numerical simulation of rough-wall heat transfer in a turbulent channel flow, Int. J. Heat Fluid Flow 22 (2001) 237–244.
[10] H. Kawamura, K. Ohsaka, H. Abe, K. Yamamoto, DNS of turbulent heat transfer in channel flow with low to

medium-high Prandtl number fluid, Int. J. Heat Fluid Flow 19 (1998) 482–491.
[11] S.L. Lyons, T.J. Hanratty, J.B. Mclaughlin, Direct numerical simulation of passive heat transfer in turbulent channel flow, Int. J. Heat Mass Transfer 34 (1991) 1149–1161.
[12] S.L. Lyons, T.J. Hanratty, J.B. Mclaughlin, Large-scale computer simulation of fully developed turbulent channel flow, Int. J. Numer. Methods Fluids 13 (1991) 999–1028.
[13] M. Germano, Turbulence: the filtering approach, J. Fluid Mech. 238 (1991) 325–336.
[14] M. Germano, U. Piomelli, P. Moin, W. Cabot, A dynamic subgrid-scale eddy viscosity model, Phys. Fluids 3 (1991) 1760–1765.
[15] P. Moin, K. Squires, W. Cabot, S. Lee, A dynamic subgrid-scale model for compressible turbulent and scalar transport, Phys. Fluids 3 (1991) 2746–2757.
[16] W-P. Wang, R.H. Pletcher, On the large eddy simulation of a turbulent channel flow with significant heat transfer, Phys. Fluids 8 (1996) 3354–3366.
[17] I. Calmet, J. Magnaudet, Large-eddy simulation of high-Schmidt number mass transfer in a turbulent channel flow, Phys. Fluids 9 (1997) 438–455.
[18] Y. Zang, R.L. Street, J.R. Koseff, A dynamic mixed subgrid-scale model and its application to turbulent recirculating flows, Phys. Fluids 5 (1993) 3186–3196.
[19] U.K. Chakravarthy, S. Menon, Linear eddy simulations of Reynolds number and Schmidt number effects on turbulent scalar mixing, Phys. Fluids 13 (2001) 488–499.
[20] J. Kim, P. Moin, Application of fractional-step method to incompressible Navier–Stokes equations, J. Comput. Phys. 59 (1985) 308–323.
[21] R. Verzicco, P. Orlandi, A finite-difference scheme for three-dimensional incompressible flows in cylindrical coordinates, J. Comput. Phys. 123 (1996) 402–414.
[22] R. Verzicco, R. Camussi, Prandtl number effects in convective turbulence, J. Fluid Mech. 383 (1999) 55–73.
[23] P. Moin, J. Kim, Numerical investigation of turbulent channel flow, J. Fluid Mech. 118 (1982) 341–377.
[24] J. Kim, P. Moin, R. Moser, Turbulence statistics in fully developed channel flow at low Reynolds number, J. Fluid Mech. 195 (1987) 133–166.
[25] H. Kreplin, H. Eckelmann, Behavior of the three fluctuating velocity components in the wall region of a turbulent boundary layer, Phys. Fluids 22 (1979) 1233–1241.
[26] F.Q. Zhong, N.S. Liu, X.Y. Lu, L.X. Zhuang, An improved dynamic subgrid-scale model for the large eddy simulation of stratified channel flow, Sci. China A 45 (2002) 888–899.
[27] N.Y. Liu, X.Y. Lu, L.X. Zhuang, A new dynamic subgrid-scale model for the large eddy simulation of stratified turbulent flows, Sci. China A 43 (2000) 391–399.
[28] C.T. Hsu, X.Y. Lu, M.K. Kwan, LES and RANS studies of oscillating flows over a flat plate, ASCE J. Eng. Mech. 126 (2000) 186–193.
[29] B.A. Kader, Temperature and concentration profiles in fully turbulent boundary layers, Int. J. Heat Mass Transfer 24 (1981) 1541–1545.
[30] Y. Nagano, M. Shimada, Development of a two-equation heat transfer model based on direct simulations of turbulent flows with different Prandtl numbers, Phys. Fluids 8 (1996) 3379–3402.